Microchemical Journal 160 (2021) 105663

Contents lists available at ScienceDirect

Microchemical Journal

journal homepage: www.elsevier.com/locate/microc

Green synthesis of $ZnO/ZnCo_2O_4$ and its application for electrochemical determination of bisphenol A

Mahnaz Amiri [a,b], Hadi Mahmoudi-Moghaddam [c,d,*]

[a] Neuroscience Research Center, Institute of Neuropharmacology, Kerman University of Medical Science, Kerman, Iran
[b] Cell Therapy and Regenerative Medicine Comprehensive Center, Kerman University of Medical Science, Kerman, Iran
[c] Environmental Health Engineering Research Center, Kerman University of Medical Sciences, Kerman, Iran
[d] Department of Environmental Health, School of Public Health, Kerman University of Medical Sciences, Kerman, Iran

ARTICLE INFO

Keywords:
BPA
Screen printed electrode
Glycyrrhiza glabra
$ZnO/ZnCo_2O_4$
Water

ABSTRACT

The present research reports the synthesis of the $ZnO/ZnCo_2O_4$ nanocomposite using a hydrothermal reaction in the presence of *Glycyrrhiza glabra* extract as one of the green precursors acting as reducing and capping agent. The scanning electron microscopy (SEM), vibrating sample magnetometry (VSM), X-ray diffraction (XRD) as well as fourier-transform infrared spectroscopy (FT-IR) have been utilized for characterizing the nanocomposite. In addition, $ZnO/ZnCo_2O_4$ has been utilized as an electrode modifier to detect bisphenol A (BPA). At the optimized condition, $ZnO/ZnCo_2O_4$/Screen printed electrode (SPE) could be employed for quantifying BPA via differential pulse voltammetry (DPV) with the linear range between 0.06 and 200.0 μM and correlation coefficient equal to 0.9985. Moreover, 0.01 μM for limit of detection (LOD) was calculated. Based on the results, our sensor showed high selectivity to BPA. Furthermore, acceptable stability and repeatability has been demonstrated in the sensor. Ultimately, $ZnO/ZnCo_2O_4$/SPE has been substantially utilized to detect BPA in the water samples.

1. Introduction

Researches have shown BPA as one of the estrogenic environmental toxins with the widespread utilization for producing poly-carbonate plastics, flame retardant, epoxy resins, etc. At the determined condition, BPA is capable of releasing into the environment from the bottles, plastics plants, packing as well as landfill leachates [1,2]. Therefore, researchers demonstrated it as one of the potent risks to the public health. It is notable that a particular volume of BPA can result in the damages to the development of brain, behavior and sexual differentiation and influence the immune functions [3]. Hence, establishing one of the simplified and sensitive methods to determine the trace amount of BPA would be of high importance. In this regard, researchers presented multiple analytical procedures to detect BPA that include liquid chromatography [4], fluorimetry [5], and enzyme-linked immuno-sorbent assay [6].

Even though these procedures have been shown adequate sensitivity and efficiency to determine BPA, numerous caveats should be resolved that include costly equipment, laborious procedure, robust pretreatment requirement and finally skilled operators [7–11]. Out of the mentioned methods, researchers largely considered electrochemical sensors as a result of their faster response rate, simplified miniaturization and convenient operation that showed their benefits in comparison to the larger instrument-based procedures [12,13]. Nevertheless, ratio of the signal to noise of the bare electrode is not adequate for determining trace level of BPA. Thus, researchers made multiple attempts via modification of the surface of the bare carbon electrode with different kinds of nanomaterials [14–16]. Ali et al. have designed a new modified SPE for detection of BPA using multiwall carbon nanotubes (MWCNTs) with β-cyclodextrin (βCD) and the detection limit of 0.013 μM was achieved [17]. In the study of Wang et al. chitosan and nickel nanoparticle/carbon nanocomposite was used as the modifier to construct an electrochemical sensor for BPA detection and LOD of 0.04 μM was reported for BPA [18]. Safavi Gerdin et al have used La^{3+}/ZnO nanoflowers for modifying SPE and the LOD value of 0.25 μM was calculated for BPA [19]. Beitollahi et al prepared a new modified SPE using MnO_2 nanorods and LOD of 0.5 μM was obtained for BPA [20]. Although some satisfactory results have been achieved for these modified electrodes but it is a challenge to develop simpler and more effective electrochemical sensor for BPA determination.

Among the metal oxides, scientists employed the cobalt oxides for the modification the surface of electrode for different electrochemical

* Corresponding author at: Environmental Health Engineering Research Center, Kerman University of Medical Sciences, Kerman, Iran (H. Mahmoudi-Moghaddam).
E-mail address: h.mahmoudi@kmu.ac.ir (H. Mahmoudi-Moghaddam).

https://doi.org/10.1016/j.microc.2020.105663
Received 26 August 2020; Received in revised form 16 October 2020; Accepted 21 October 2020
Available online 26 October 2020

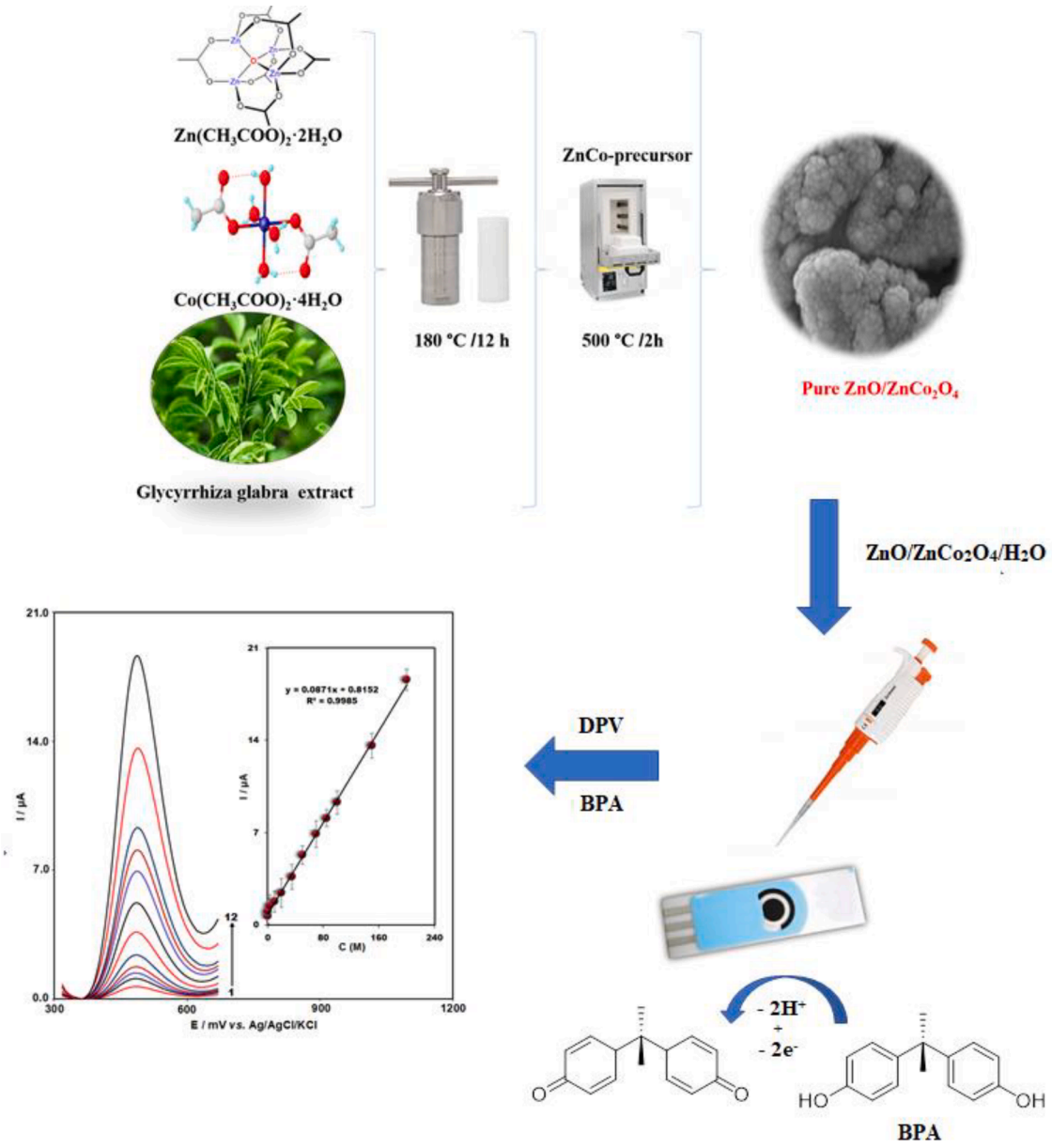

Scheme 1. Development of the modified sensor for determination of BPA.

utilizations [21]. Nonetheless, as a result of their simplified aggregation and low electrical conductivity, they show a comparatively lower electro-catalytic performances in comparison to the metal oxide-based electro-catalysts [22]. It is notable that a combination of the cobalt oxides with the other transition metal oxides has been largely considered because of their reasonable electronic conductivity, reversible capacity, and structural stability. Especially, the cobalt-based metal oxides like $MnCo_2O_4$, $ZnCo_2O_4$, $NiCo_2O_4$ as well as $FeCo_2O_4$ have been regarded as the most encouraging options for the electrode substances in sensing the analytes. Amongst the cobalt-based metal oxides, the zinc cobaltite with a cubic spinel structure ($ZnCo_2O_4$) has been considered an encouraging electrode substance for electrochemical sensors that is one of the largely investigated topics as a result of its changeable oxidation state, very good electrochemical features, inexpensiveness, and environmental-friendly nature [23,24].

Additionally, scientists have been considerably attracted by significant sensing features of the ZnO nano-particles (NPs) such as non-toxicity, higher surface area, very good bio-compatibility, electrochemical activity and chemical stability for developing utilizations, particularity, in the electrochemical sensors [25].

With regard to this notion, we combined $ZnCo_2O_4$ and ZnO for preparing a $ZnO/ZnCo_2O_4$ composite, as one of the novel hybrid electrode materials, to selectively detect BPA. It is unfortunate that multiple nanocomposite synthesis methods entail using detrimental chemicals or higher energy requirements that would be highly hard and demand useless treatments. Overall, the green synthesis of NPs indicates advancements over other methods because of their simplicity, environmental-friendliness, inexpensiveness, and reproducibility and most of the time result in the preparation of more stable substances [26,27]. Hence, this study addressed the synthesis of the $ZnO/ZnCo_2O_4$ composite based on the green strategy and *Glycyrrhiza glabra* extract has been utilized as the reducing and capping agent. In addition, we examined electrochemical and morphological features of $ZnO/ZnCo_2O_4$ nano-composite. Finally, nano-composite exhibited good electrochemical activities for oxidizing BPA in comparison with the bare SPE (Scheme 1).

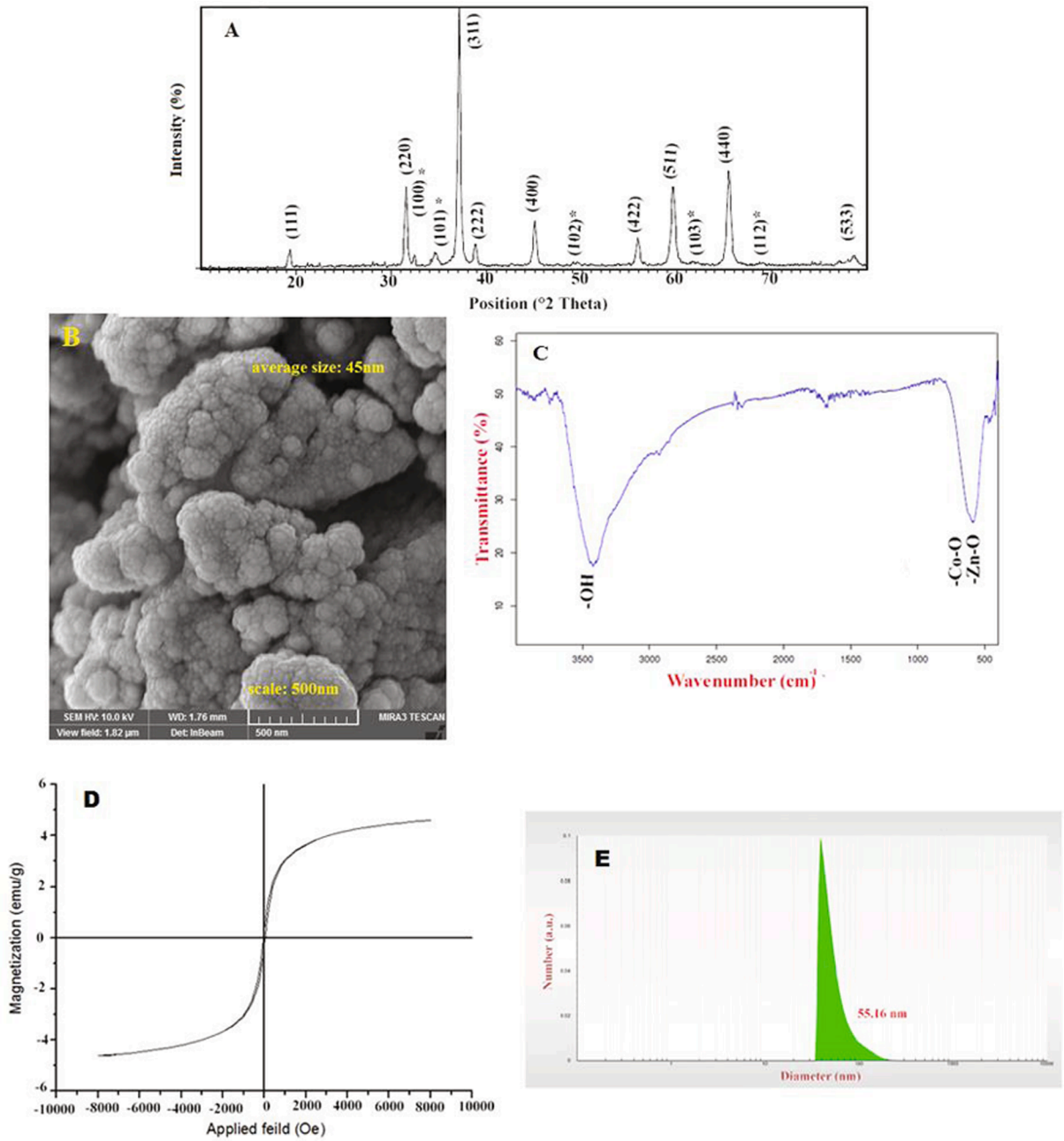

Fig. 1. A) XRD, B) SEM image, C) FT-IR spectrum, D) VSM magnetization curve and E) size analyzer graph of $ZnO/ZnCo_2O_4$.

2. Material and methods

2.1. Chemicals and reagents

According to the research design, BPA, $Zn(CH_3COO)_2{\cdot}2H_2O$, $Co(CH_3COO)_2{\cdot}4H_2O$ (98%< purity) has been bought from Sigma Company. The standard stock solution of 1.0 mM BPA has been procured by 50% (V/V) ethanol and distilled water solution. Moreover, 0.1 M phosphate buffer solution (PBS) with distinct pH-values (3.0 to 9.0) has been procured via mixing KH_2PO_4 and K_2HPO_4 stock solution and setting pH with NaOH (0.5 M) and H_3PO_4 (1 M). Each reagent has been of analytical grade and utilized without additional treatments. The solution has been procured with the use of the double distilled water.

In the next stage, electrochemical experiments have been performed with a Metrohm 797 electrochemical analyzer monitored by a microcomputer using Metrohm 797 computrace software. Notably, a graphite as the working electrode, a silver as the pseudo-reference electrode as well as a graphite as counter electrode have been selected as the parts forming the screen-printed electrode (SPE) (Drop-Sens, DRP-110, Spain).

The nanostructure were characterized by XRD, FT-IR (Nicolet Magna-550 spectrometer), VSM (Meghnatis Kavir Kashan Company, Kashan, Iran), Nanosizer (Cordouan: France) as well as FE-SEM (ZEISS, SIGMA VP-500: Germany) to analyze the morphology of the particle.

2.2. Preparing Glycyrrhiza glabra

In this stage, *Glycyrrhiza glabra* root has been collected and distilled water has been used to thoroughly wash it. Then, we dried it in an oven at 40 °C for 24 h and ground it. After that, the powder passed a 100-mesh sieve and kept in a desiccator. The extracts have been procured by macerating with the distilled water at the room temperature (the

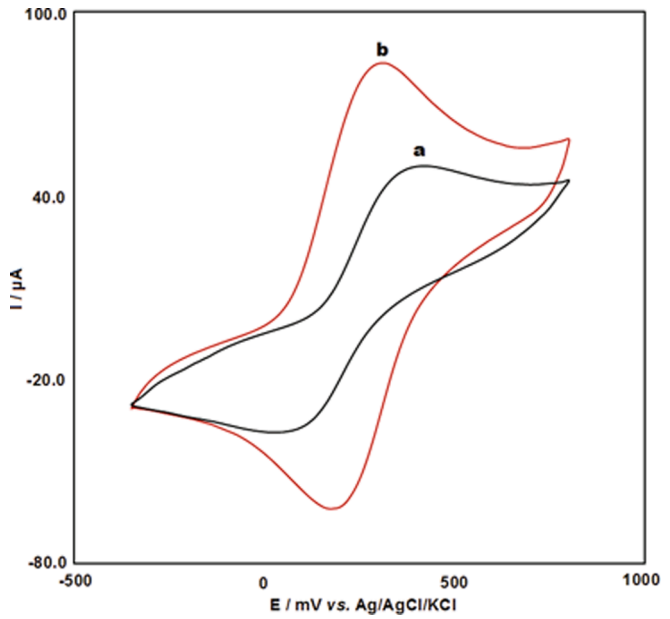

Fig. 2. Cyclic voltammograms of 1 mM $[Fe(CN)_6]^{3-}/^{4-}$ in 0.1 M KCl at (a) SPE, (b) $ZnO/ZnCo_2O_4$/SPE.

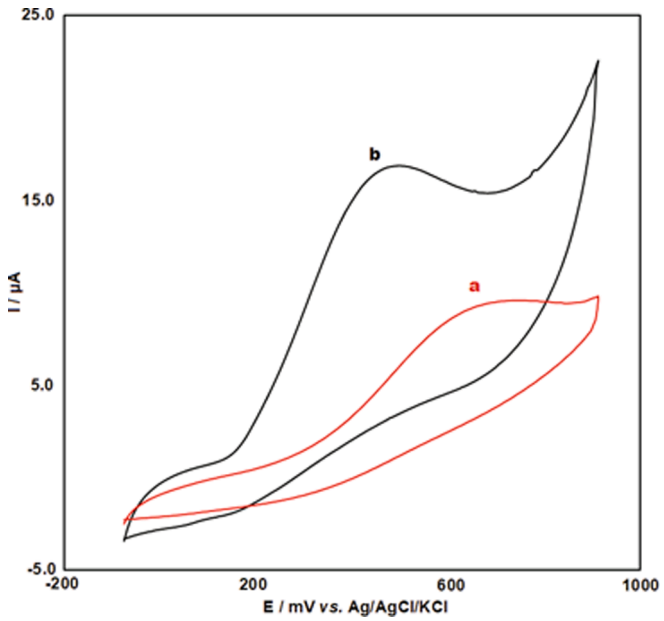

Fig.3. Cyclic voltammograms of (a) bare SPE and (b) $ZnO/ZnCo_2O_4$/SPE in the presence of 150 µM BPA in 0.1 M PBS (pH = 7.0) at the scan rate of 50 mVs^{-1}.

ratio of herbal-to-water equal 1:1 (w/w)) with the constant stirring over 48 h. Upon the filtration, the raw extracts have been evaporated at 40 °C at a lower pressure and thus extraction yield has been specified. Finally, the extract has been kept at 4 °C for additional uses [28].

2.3. Preparing $ZnO/ZnCo_2O_4$ nanocomposite

A 2-phase path has been considered for the preparation of the pure $ZnO/ZnCo_2O_4$ nanocomposite. Therefore, in the first hydrothermal stage, the mixed solution has been procured via dissolving Zn $(CH_3COO)_2{\cdot}2H_2O$ and $Co(CH_3COO)_2{\cdot}4H_2O$ with 2:1 stoichiometric ratio in 30 mL distilled water at 30 °C. After that a specific volume of the *Glycyrrhiza glabra* extract aqueous solution has been added drop-by-drop by vigorous stirring. Next, this solution has been sealed in a 50 mL Teflon lined stainless steel auto-clave and stored at 180 °C for 12 h. When it has been cooled down to the room temperature, we gathered the final product through centrifugation and used ethanol and distilled water to wash it for several times. Then, it has been dried at 70 °C for twelve hours for obtaining ZnCo-precursor. For the next phase, we put the procured precursor in the furnace and annealing has been performed at 500 °C in air for two hours for obtaining a pure $ZnCo_2O_4$ sample. For synthesizing the ZnO-decorated $ZnCo_2O_4$, the same procedure in the presence of the pure $ZnCo_2O_4$ has been utilized; however, just volume of $Zn(CH_3COO)_2{\cdot}2H_2O$ (nearly 2 times) enhanced in the absence of the cobalt salt in a hydrothermal phase. It has been found that the green (environmental-friendly) chemical methods are the procedures emphasizing the development of the free organic solvents and reduction of the energy taking procedures [29].

2.4. Electrode preparation

The $ZnO/ZnCo_2O_4$ nanocomposite have been employed for coating the bare SPE. Therefore, 1 mg of $ZnO/ZnCo_2O_4$ homogenized with ultrasonication for 30 min in 1 mL aqueous solution, then 2 µl of aliquots of $ZnO/ZnCo_2O_4/H_2O$ suspension solution has been poured at the surface of the carbon working electrode. Consequently, the solvent has been put aside for evaporating at the room temperature.

2.5. Preparing the real samples

We collected drinking, bottled, river and waste water in Kerman (Iran), so a 0.22 µm membrane has been used to filter the water samples and pH has been set to 7.0 with 0.1 M PBS solution.

3. Result and discussion

3.1. Characterizing the $ZnO/ZnCo_2O_4$ nanocomposite

XRD analysis has been used to examine the structural description of the $ZnCo_2O_4/ZnO$ nanocomposite (Fig. 1A). It is notable that * refers to the respective diffraction standard cards of ZnO and no symbol stands for $ZnCo_2O_4$. Moreover, $ZnCo_2O_4$ crystal structure has been verified through 220, 331, 222, 400, 422, 511 and 440 peaks (spinel cubic $ZnCo_2O_4$, No. 23-1390). However, the residual peaks have been indexed in wurtzite ZnO (JCPDS No. 42-1451) [30]. As seen, XRD outputs presents total transformation of Zn–Co precursors into the ZnO and $ZnCo_2O_4$ crystals following a calcination procedure. In addition, sharp and intense peaks demonstrate the complete and crystallization of the sample. We did not observe any peak of impurity that verifies a desirable purity of the nanocomposite. Average size of the samples of nanocrystallite equaled 35 ± 1 nm computed by Debye Scherer's equation [31]

$$(D = k\lambda/\beta\cos\theta) \quad (1)$$

here D represents the size of the NPs crystallite and k stands for the shape factor (0.9). Moreover, λ refers to wave-length of the X-ray (1.54 Å) Cu Kα radiation and θ represents Bragg angle form 2θ value of the intensity peak from the XRD pattern. Finally, β implies a full width half maximum of diffraction from XRD pattern of the NPs.

The SEM has been used to examine the morphology of the pure $ZnCo_2O_4/ZnO$. The non-agglomerated and spherical particles can be seen in the Fig. 1B. The average size of nanostructures is about 45 ± 10 nm.

FT-IR spectra of the procured samples have been shown in Fig. 1C. As seen, the wide strong IR adsorption band (greater than 3000 cm^{-1}) verified the presence of OH stretching mode as a result of the water adsorption on the sample surfaces. Moreover, the absorption bands have been seen below 580 cm^{-1}, which demonstrated Zn-O and Co-O

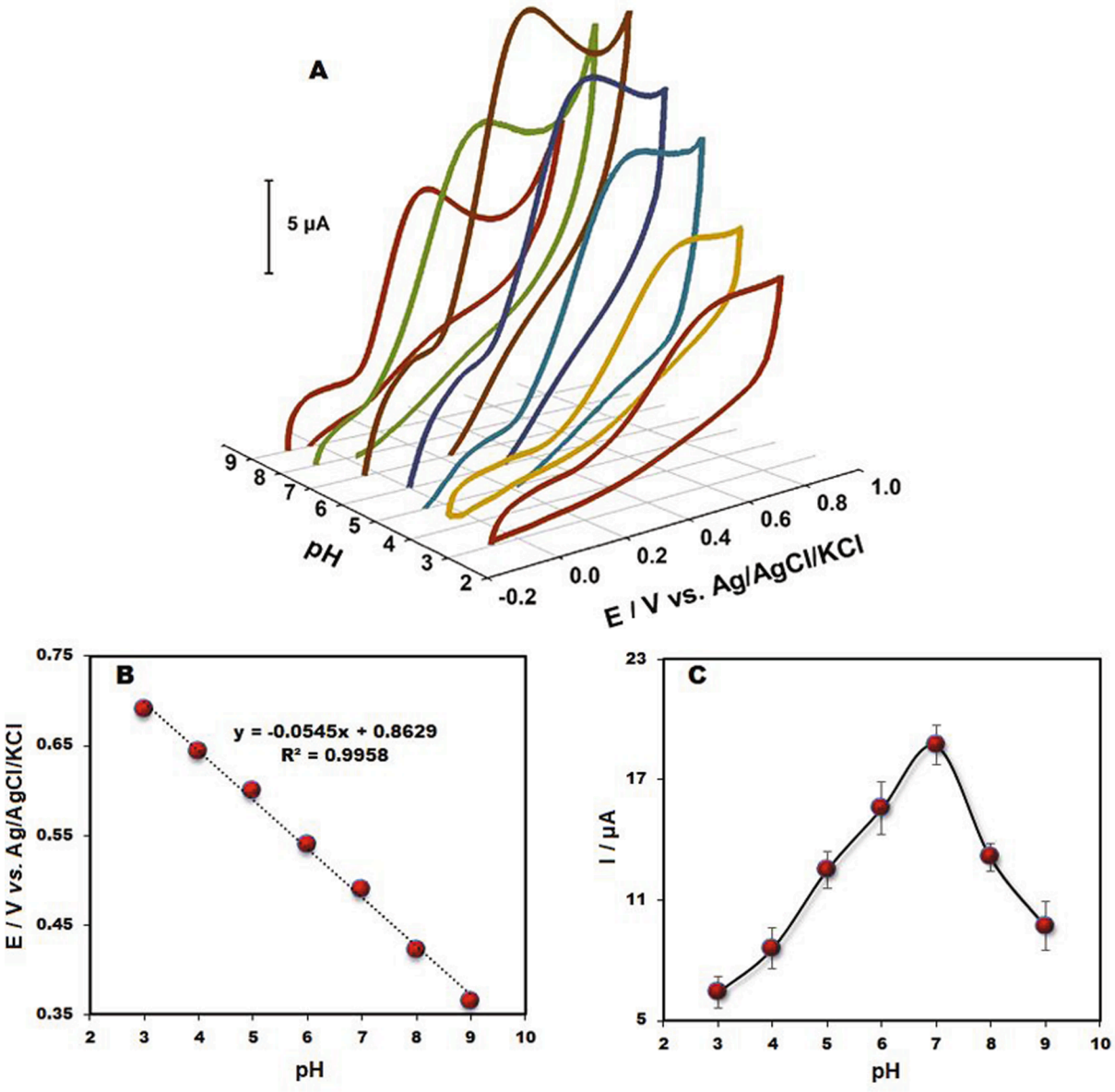

Fig. 4. (A) CV voltammograms of 200.0 μM BPA at the ZnO/$ZnCo_2O_4$/SPE in PBS solution in the pH range 3–9. (B) The pH plot vs. peak potential (E_{pa}) and (C) The effect of pH on the I_{pa} of BPA.

stretching vibrations. Hence, remaining absorption peaks seen at 1645 cm^{-1} could be ascribed to the bending vibration H-O–H (water) [32]. Furthermore, the nanocrystal magnetic stuff has been examined by a vibrating sample magneto-meter at 300 K (Fig. 1D) and saturation magnetization (Ms) of 3.49 emu g^{-1} obtained. Overall, zinc cobaltite at the room temperature proved a para-magnetic nature due to its normal spinel structure. However, opportunities of the partial inversion are found out of the $ZnCo_2O_4$ NPs, which result in coupling of the cations of octahedral and tetrahedral sites and enhance incidence of the super-paramagnetic coupling [33]. Finally, the coupling impacts have been shown to be size-dependent. For reaching more accurate information of the lower agglomeration of the samples, we utilized the nano-sizer analysis (Fig. 1E). Finally, average hydrodynamic diameter of the samples (55.16 nm), showing good fitness of the auto-correlation functions with Pade Laplace analyses.

3.2. Electrochemical properties of modified electrode

For assessing the electrochemical properties of the sensor, $[Fe(CN)6]^{3-/4-}$ couples have been utilized as the electrochemical probe. Then, electrochemical performance of ZnO/$ZnCo_2O_4$/SPE has been assessed in 0.1 mM $[Fe(CN)6]^{3-/4-}$ redox probe. As seen in Fig. 2, redox peaks remarkably improved at ZnO/$ZnCo_2O_4$/SPE (83.1 μA) in comparison to bare SPE (48.9 μA). Such a situation can be caused by accelerating the electron transfer and larger surface area of ZnO/$ZnCo_2O_4$ that causes the increased current responses. It has been found that peak to peak potential (ΔE_p) is 121 mV and 253 mV at the ZnO/$ZnCo_2O_4$/SPE and bare SPE respectively. With regard to smaller value of ΔE_p at the ZnO/$ZnCo_2O_4$/SPE, the procedure of the electron transfer proceeds quickly and is quasi-reversible, reflecting the electrode capability to produce a good micro-environment for undergoing the simplified electron-transfer reaction.

3.3. Electrochemical behavior of BPA at ZnO/$ZnCo_2O_4$/SPE

In order to investigate BPA electrochemical behavior at the modified SPE, we compared oxidation potential and oxidation current in 0.1 M PBS at pH of 7.0 consisting of 150 μM BPA. Fig. 3 demonstrates cyclic

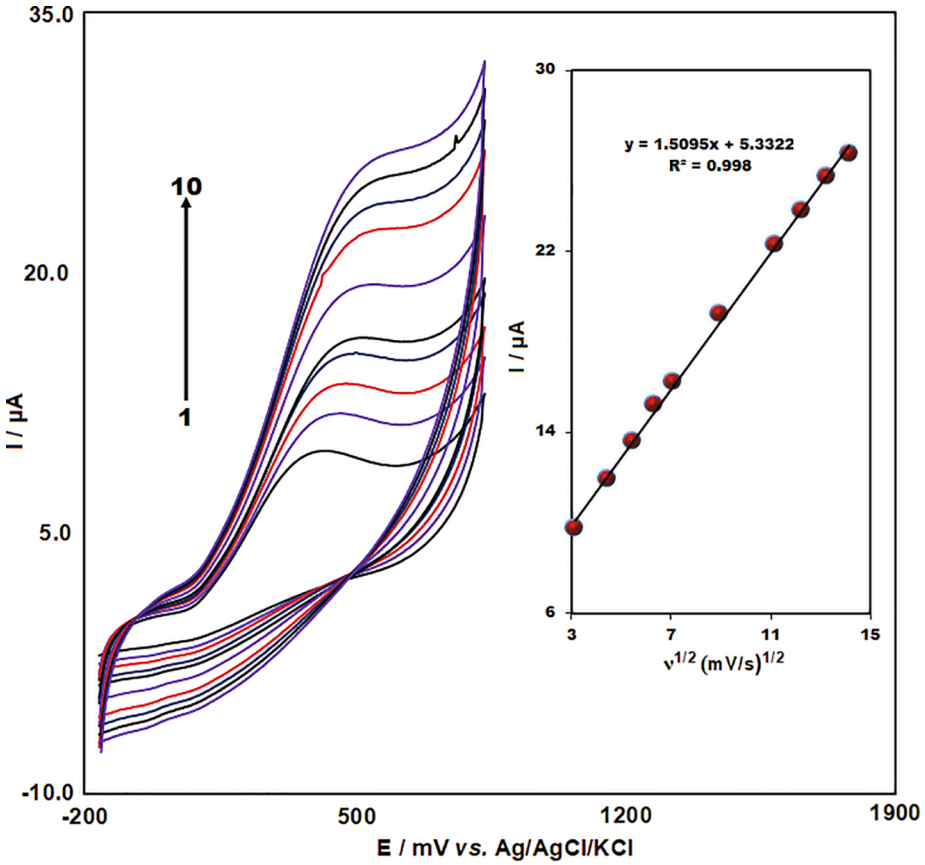

Fig. 5. CVs of 100.0 μM BPA through ZnO/$ZnCo_2O_4$/SPE in 0.1 M PBS (pH of 7.0) at the scan rates of 10, 20, 30, 40, 50, 80, 125, 150, 175 and 200 mV s^{-1} (numbers 1–10, respectively). Inset: I versus $\nu^{1/2}$.

voltammograms for modified and bare SPE. As seen, a clear oxidation peak of BPA has been appeared at 495 mV for modified (curve b) and 680 mV for bare SPE (curve a). Any related reduction peak has been not observed in the reverse scan, indicating irreversibility of electrochemical oxidation procedure of BPA. In comparison to bare electrode (9.4 μA), peak current on ZnO/$ZnCo_2O_4$/SPE experienced a considerable enhancement (16.8 μA). Therefore, the obtained outputs indicated ability of ZnO/$ZnCo_2O_4$/SPE for accelerating BPA electro-oxidation that can be ascribed to a substantial introduction of ZnO and specific features of $ZnCo_2O_4$ like highly efficient specific surface areas and more reasonable electric conductivity.

3.4. Effect of pH

In this stage, we used CV to examine pH impact on the oxidation of 200 μM BPA at the modified electrode in a pH range between 3 and 9 (Fig. 4A). Therefore, oxidation peak potential (E_{pa}), switched to the negative potential values with the ascending pH, which has been followed by a linear association with equation of E_{pa} (V) = − 0.0545 pH + 0.8629, reflecting that protons have a direct contribution to BPA oxidation (Fig. 4B). Then, the slope value has been obtained −54.5 mV that was near the theoretical value of 59 mV which implies the equality of the number of the electron as well as proton in oxidation of BPA (Scheme S2). As shown in Fig. 4C, current intensity enhanced slowly from pH of 3.0 to 7.0, and consequently declined; so, we chose 0.1 M PBS as a supporting electrolyte with the pH value of 7.0 for additional investigation for maximizing sensitivity to detect BPA.

3.5. Scan rate effect

For examining the reaction kinetics, we utilized CV to determine impact of the scan rate on the oxidation peaks current of BPA at ZnO/$ZnCo_2O_4$/SPE. Fig. 5 indicates impact of the scan rate on electrochemical behavior of ZnO/$ZnCo_2O_4$/SPE toward BPA. As seen, anodic peak currents enhanced with increasing scan rate from 10 to 200 mVs^{-1}, reflecting the kinetics limitation of electrochemical procedure. In addition, the square root of the scan rate vs. the oxidation peak current plot with the linear regression equation of E_{pa} (V) = 1.509x + 5.33 (R^2 = 0.998) was obtained (Fig. 5-inset), showing oxidation procedure of BPA at ZnO/$ZnCo_2O_4$/SPE has been a diffusion-controlled electron transfer procedure.

3.6. Chronoamperometry analyzing

The chrono-amperometry of ZnO/$ZnCo_2O_4$/SPE has been performed for studying BPA oxidation (at the potential of 0.49 V versus the reference electrode) and estimating BPA diffusion coefficient in 0.1 M phosphate buffer solution (Fig. 6). Moreover, Cottrell's equation may be utilized for explaining the current response (I) for diffusion-limited electrocatalytic procedures of the electro-active substances.

$$I = nFAC_bD^{1/2}\pi^{-1/2}t^{-1/2} \quad (2)$$

where D (cm^2s^{-1}) represents diffusion coefficient of analyte and F refers to Faraday constant. In addition, C_b stands for bulk concentration of analyte (mol cm^{-3}) and n indicates number of the electrons exchanged in each reactant molecule. Moreover, A represents the electrode surface area. Hence, experimental plots of I versus $t^{-1/2}$ have been drawn and the fitted lines slopes have been specified at different BPA concentrations (Fig. 6-inset A). Then, the slope of the attained straight lines has been drawn against BPA concentration. According to the Cottrell equation and the observed slops in the Fig. 6-inset B, BPA diffusion coefficient has been approximated to be 1.05 × 10^{-5} cm^2 s^{-1} in this

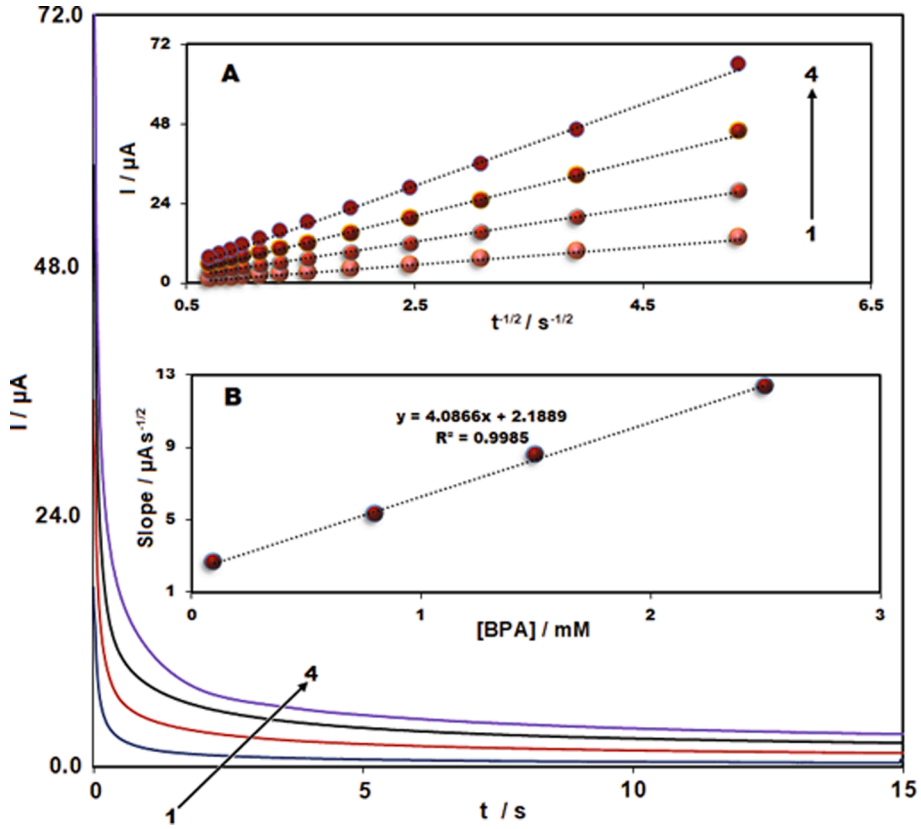

Fig. 6. Chronoamperograms achieved for diverse concentrations of BPA at $ZnO/ZnCo_2O_4$/SPE in 0.1 M PBS (pH 7.0). Numbers 1–4 is corresponding to 0.1, 0.8, 1.5, and 2.5 mM of BPA Insets: (a) I plot versus $t^{-1/2}$ achieved from chronoamperograms 1–4 and (b) The straight-line slope plot versus BPA concentrations.

study.

3.7. Calibration curve and limit of detection

Based on the optimum experimental condition, DPV has been used to analyze BPA standard solutions. Fig. 7 represents DPV response of SPE toward various concentrations of BPA. As seen, peak currents experienced a linear rise by enhancing the concentration of BPA in the range between 0.06 and 200.0 μM with a linear regression equation of I_{pa} (μA) = 0.0871x + 0.8152 (R^2 = 9985) and finally, 0.01 μM as the LOD value was calculated (S/N = 3) (Fig. 7-inset). For comparing functions of other sensors with this new sensor, Table 1 reports the analytical outputs of these sensors. In comparison to some sensors, this new electrochemical sensor displayed comparable analytical functions like wider linear range and lower LOD.

3.8. Stability and repeatability

For checking repeatability, one modified SPE has been utilized for detecting BPA (Fig. S1-A). A nearly similar outcome has been found in 10 iterated tests with 3.42% relative standard deviation (RSD) for 50.0 μM of BPA, reflecting reasonable repeatability of this new sensor. Moreover, we kept electrode at the room temperature for four weeks and detected the BPA two times weekly in order to examine lengthy stability of this sensor (Fig. S1-B). Then, it retained 94% of its initial response, showing acceptable storage stability of SPE.

3.9. Interference study

According to the research design, interference study has been done in presence of 10.0 μM BPA using DPV. Based on the results, for 100-fold concentration of Mg^{2+}, Ca^{2+}, K^+, Zn^{2+}, Al^{3+}, Fe^{3+}, NO_3^-, and SO_4^{2-}, changes in the anodic currents have been lower than 4% that showed they did not have any effect on the BPA detection. In addition, 50-fold concentration of hydroquinone, 2-Nitrophenol, 4-Nitrophenol, pyrocatechol, glucose, lactose, phenol, catechol and ascorbic acid did not show any impact on BPA detection with <5% I_{pa} changes (Fig. S2). Therefore, this new sensor showed good selectivity towards BPA.

3.10. BPA determination in the real samples

This new sensor has been substantially utilized to detect BPA in the different water samples that have been procured through a method described in Part 2.5. These samples have been spiked with three distinct concentrations of BPA solution and 3 replicate measurements have been carried out at all concentration. Table 2 presents experimental outputs. Additionally, recovery values equaled 95%-104.2% with RSD of 2.0 to 3.8%, reflecting the sensor is capable of successful utilization to detect BPA in the real samples.

In the next stage, the results of BPA determination using $ZnO/ZnCo_2O_4$ were compared with high performance liquid chromatography (HPLC) method in water samples. Therefore, the student's t-test were applied to compare the outputs of electrochemical and HPLC methods. As shown in Table 3, the calculated t-values were smaller than the t-critical value at a confidence interval (CI) of 95%, indicating that there is no significant difference between the proposed method and the HPLC method.

4. Conclusion

In summary, magnetic nanocomposites have been successfully synthesized by a green reducing agent, *Glycyrrhiza glabra* extract, using hydrothermal route. Moreover, this research presented one of the new electrochemical sensor for BPA on the basis of the $ZnO/ZnCo_2O_4$

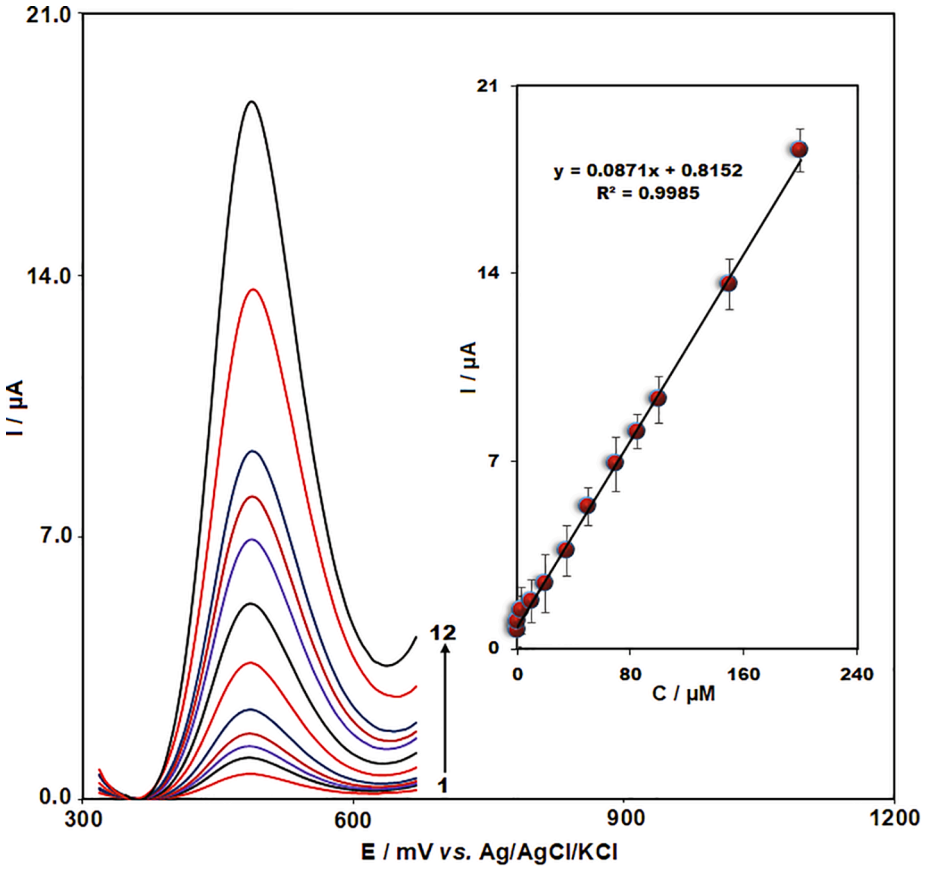

Fig. 7. Differential pulse voltammograms recorded for $ZnO/ZnCo_2O_4$/SPE in the 0.1 M PBS (pH of 7.0) consisting of diverse concentrations of BPA. Values 1–12 are corresponding to 0.06, 0.5, 3.0, 10.0, 20.0, 35.0, 50.0, 70.0, 85.0, 100.0, 150.0 and 200.0 µM of BPA. Inset: I plot as a function of BPA concentration.

Table 1
Comparison of the efficiency of different electrodes in the determination of BPA.

Electrode	Linear range (µM)	LOD (µM)	Ref.
CNT/TiO_2PE	1.0–600	3	[34]
Pt/PDDADMP/GCE	5–30 & 10–60	0.6	[35]
PME/GR-CPE	9.0–1000	0.0105	[36]
GN/GCE	0.1–100	0.035	[37]
MOF-508a/GCE	0.1–700.0	0.03	[38]
NiNPs/NCN/CS/GCE	0.1–2.5 and 2.5–15.0	0.045	[18]
Ce-MOF-ERGO/GCE	0.003 to 10	0.0019	[39]
La^{3+}-doped Co_3O_4 nanocube/SPE	0.5–900.0	0.061	[40]
Fe_3O_4NPs/SPE	0.03 and 700.0	0.01	[41]
DPNs/SPE	0.01–1 and 1–300	0.0066	[42]
MCM-41/CPE	0.088–0.22	38	[43]
$ZnO/ZnCo_2O_4$/SPE	0.06–200.0	0.01	This study

Table 2
Results of the determination of BPA in real samples. (n = 3).

Sample	Spiked (µM)	Found (µM)	Recovery (%)	RSD (%)
Drinking water	0.0	N.D	–	–
	5.0	5.2	104.0	2.9
	10.0	9.8	98.0	2.4
	15.0	14.4	96.0	2.5
River water	0.0	N.D	–	–
	6.0	6.2	103.3	3.2
	12.0	12.5	104.1	2.9
	18.0	17.5	97.2	2.7
Bottled water	0.0	1.1	–	3.8
	5.0	5.8	95.0	3.1
	15.0	16.6	103.1	2.5
	25.0	25.7	98.4	2.1
Waste water	0.0	11.2	–	3.4
	10.0	22.1	104.2	3.0
	20.0	30.7	98.4	2.0
	30.0	40.3	97.8	2.2

nanocomposite. This modified SPE showed a number of benefits like low LOD, acceptable repeatability and stability, simplified procurement procedure as well as very good selectivity. In addition, reasonable recovery outputs have been obtained in determining BPA in the real samples.

CRediT authorship contribution statement

Mahnaz Amiri: Software, Investigation, Writing - original draft, Methodology. **Hadi Mahmoudi-Moghaddam:** Supervision, Conceptualization, Methodology, Investigation, Resources, Writing - review & editing.

Declaration of Competing Interest

The authors declare that they have no known competing financial interests or personal relationships that could have appeared to influence the work reported in this paper.

Acknowledgment

This work was supported by Kerman University of Medical Sciences under grant number 98001016 and the code of research ethics certificate IR.KMU.REC.1398.649.

Table 3
Determination of BPA in water samples using modified electrode and HPLC method (n = 3).

Sample	Added (μM)	Found (μM)		Recovery%		t value	
		DPV	HPLC	DPV	HPLC	Exp.	Critical (95% CI)
Bottled water	–	1.12 ± 0.04	0.99 ± 0.20	–	–	1.1040	2.776
	5.00	5.82 ± 0.18	5.88 ± 0.30	95.0	98.1	0.2970	2.776
	15.00	16.65 ± 0.41	16.77 ± 0.11	103.1	104.8	0.4925	2.776
	25.00	25.74 ± 0.54	25.63 ± 0.71	98.5	98.6	0.2136	2.776
Waste water	–	11.23 ± 0.38	11.42 ± 0.12	–	–	0.8258	2.776
	10.00	22.09 ± 0.66	22.29 ± 0.91	104.2	104.0	0.3082	2.776
	20.00	30.70 ± 0.61	30.88 ± 0.34	98.4	98.2	0.4464	2.776
	30.00	40.32 ± 0.88	41.8 ± 0.62	97.8	101.0	2.3813	2.776

Appendix A. Supplementary data

Supplementary data to this article can be found online at https://doi.org/10.1016/j.microc.2020.105663.

References

[1] B. Suyamud, P. Thiravetyan, G.M. Gadd, B. Panyapinyopol, D. Inthorn, Bisphenol A removal from a plastic industry wastewater by Dracaena sanderiana endophytic bacteria and Bacillus cereus NI, Int. J. Phytoremediation 22 (2020) 167–175, https://doi.org/10.1080/15226514.2019.1652563.

[2] L. or Chailurkit, K. Srijaruskul, B. Ongphiphadhanakul, Bisphenol A in canned carbonated drinks and plastic-bottled water from supermarkets, Expo. Heal. 9 (2017) 243–248. doi: 10.1007/s12403-016-0235-5.

[3] K. Pelch, J.A. Wignall, A.E. Goldstone, P.K. Ross, R.B. Blain, A.J. Shapiro, S. D. Holmgren, J.H. Hsieh, D. Svoboda, S.S. Auerbach, F.M. Parham, S.A. Masten, V. Walker, A. Rooney, K.A. Thayer, A scoping review of the health and toxicological activity of bisphenol A (BPA) structural analogues and functional alternatives, Toxicology 424 (2019), 152235, https://doi.org/10.1016/j.tox.2019.06.006.

[4] P. Gallo, I. Di Marco Pisciottano, M. Fattore, M.G. Rimoli, S. Seccia, S. Albrizio, A method to determine BPA, BPB, and BPF levels in fruit juices by liquid chromatography coupled to tandem mass spectrometry, Food Addit. Contam. – Part A Chem. Anal. Control. Expo. Risk Assess. 36 (2019) 1871–1881, https://doi.org/10.1080/19440049.2019.1657967.

[5] Y.F. Zhuang, G.P. Cao, J.Y. Mao, B.L. Liu, Determination of bisphenol A by synchronous fluorimetry using procaine hydrochloride as self-quenching fluorescence probe, J. Appl. Spectrosc. 85 (2019) 1094–1100, https://doi.org/10.1007/s10812-019-00764-x.

[6] Y. Lu, J.R. Peterson, J.J. Gooding, N.A. Lee, Development of sensitive direct and indirect enzyme-linked immunosorbent assays (ELISAs) for monitoring bisphenol-A in canned foods and beverages, Anal. Bioanal. Chem. 403 (2012) 1607–1618, https://doi.org/10.1007/s00216-012-5969-8.

[7] L.D. Nguyen, T.M. Huynh, T.S.V. Nguyen, D.N. Le, R. Baptist, T.C.D. Doan, C. M. Dang, Nafion/platinum modified electrode-on-chip for the electrochemical detection of trace iron in natural water, J. Electroanal. Chem. (2020), 114396, https://doi.org/10.1016/j.jelechem.2020.114396.

[8] H. Cheng, W. Weng, H. Xie, J. Liu, G. Luo, S. Huang, W. Sun, G. Li, Au-Pt@Biomass porous carbon composite modified electrode for sensitive electrochemical detection of baicalein, Microchem. J. 154 (2020), 104602, https://doi.org/10.1016/j.microc.2020.104602.

[9] H.M. Moghaddam, H. Beitollahi, G. Dehghannoudeh, H. Forootanfar, A label-free electrochemical biosensor based on carbon paste electrode modified with graphene and ds-DNA for the determination of the anti-cancer drug tamoxifen, J. Electrochem. Soc. 164 (2017) B372–B376, https://doi.org/10.1149/2.0561707jes.

[10] H.M. Moghaddam, Electrocatalytic determination of carbidopa and acetaminophen using a modified carbon nanotube paste electrode, Int. J. Electrochem. Sci. 6 (2011) 6557–6566.

[11] S. Tajik, H. Mahmoudi-Moghaddam, H. Beitollahi, Screen-printed electrode modified with La 3+-doped Co 3 O 4 nanocubes for electrochemical determination of hydroxylamine, J. Electrochem. Soc. 166 (2019) B402–B406, https://doi.org/10.1149/2.0491906jes.

[12] A. Soleh, P. Kanatharana, P. Thavarungkul, W. Limbut, Novel electrochemical sensor using a dual-working electrode system for the simultaneous determination of glucose, uric acid and dopamine, Microchem. J. 153 (2020), 104379.

[13] X. Guo, H. Yue, S. Song, S. Huang, X. Gao, H. Chen, P. Wu, T. Zhang, Z. Wang, Simultaneous electrochemical determination of dopamine and uric acid based on MoS2nanoflowers-graphene/ITO electrode, Microchem. J. 154 (2020), 104527.

[14] J. Zou, G.-Q. Zhao, J. Teng, Q. Liu, X.-Y. Jiang, F.-P. Jiao, J.-G. Yu, Highly sensitive detection of bisphenol A in real water samples based on in-situ assembled graphene nanoplatelets and gold nanoparticles composite, Microchem. J. 145 (2019) 693–702.

[15] H.M. Moghaddam, M. Malakootian, H. Beitollah, P. Biparva, Nanostructured base electrochemical sensor for determination of sulfite, Int. J. Electrochem. Sci. 9 (2014) 327–341.

[16] H. Beitollahi, H. Mahmoudi-Moghaddam, S. Tajik, S. Jahani, A modified screen printed electrode based on La 3+ -doped Co 3 O 4 nanocubes for determination of sulfite in real samples, Microchem. J. 147 (2019) 590–597, https://doi.org/10.1016/j.microc.2019.03.031.

[17] M.Y. Ali, A.U. Alam, M.M.R. Howlader, Fabrication of highly sensitive Bisphenol A electrochemical sensor amplified with chemically modified multiwall carbon nanotubes and β-cyclodextrin, Sensors Actuators B Chem. 320 (2020), 128319, https://doi.org/10.1016/j.snb.2020.128319.

[18] Y. Wang, C. Yin, Q. Zhuang, An electrochemical sensor modified with nickel nanoparticle/nitrogen-doped carbon nanosheet nanocomposite for bisphenol A detection, J. Alloys Compd. 827 (2020), 154335, https://doi.org/10.1016/j.jallcom.2020.154335.

[19] H. Safavi Gerdin, H. Sarhadi, S. Tajik, Determination of bisphenol A in real samples using modified graphite screen-printed electrode, Int. J. Environ. Anal. Chem. (2020) 1–10.

[20] H. Beitollahi, S. Tajik, S. Jahani, F.G. Najed, MnO2 nanorods modified screen printed electrode as a novel voltammetric sensor for specific detection of bisphenol A, Anal. Bioanal. Electrochem. 10 (2018) 1108–1119.

[21] S. Zhang, X. Wen, M. Long, J. Xi, J. Hu, A. Tang, Fabrication of CuO/Cu/TiO2 nanotube arrays modified electrode for detection of formaldehyde, J. Alloys Compd. 829 (2020), 154568, https://doi.org/10.1016/j.jallcom.2020.154568.

[22] A.M. Fekry, M. Shehata, S.M. Azab, A. Walcarius, Voltammetric detection of caffeine in pharmacological and beverages samples based on simple nano-Co (II, III) oxide modified carbon paste electrode in aqueous and micellar media, Sensors Actuators, B Chem. 302 (2020), 127172, https://doi.org/10.1016/j.snb.2019.127172.

[23] Y. Li, Y. Chu, Y. Li, C. Ma, L. Li, A novel electrochemiluminescence biosensor: Inorganic-organic nanocomposite and ZnCo2O4 as the efficient emitter and accelerator, Sensors Actuators, B Chem. 303 (2020), 127222, https://doi.org/10.1016/j.snb.2019.127222.

[24] N. Zhang, Y. Lu, Y. Fan, J. Zhou, X. Li, S. Adimi, C. Liu, S. Ruan, Metal–organic framework-derived ZnO/ZnCo2O4 microspheres modified by catalytic PdO nanoparticles for sub-ppm-level formaldehyde detection, Sensors Actuators, B Chem. 315 (2020), 128118, https://doi.org/10.1016/j.snb.2020.128118.

[25] S.J. Malode, P.K. Keerthi, N.P. Shetti, R.M. Kulkarni, Electroanalysis of carbendazim using MWCNT/Ca-ZnO modified electrode, Electroanalysis 32 (2020) 1590–1599, https://doi.org/10.1002/elan.201900776.

[26] M.S. Mohseni, M.A. Khalilzadeh, M. Mohseni, F.Z. Hargalani, M.I. Getso, V. Raissi, O. Raiesi, Green synthesis of Ag nanoparticles from pomegranate seeds extract and synthesis of Ag-Starch nanocomposite and characterization of mechanical properties of the films, Biocatal. Agric. Biotechnol. 25 (2020), 101569, https://doi.org/10.1016/j.bcab.2020.101569.

[27] P. Mondal, A. Anweshan, M.K. Purkait, Green synthesis and environmental application of Iron-based nanomaterials and nanocomposite: a review, Chemosphere (2020), 127509, https://doi.org/10.1016/j.chemosphere.2020.127509.

[28] M. Amiri, A. Akbari, M. Ahmadi, A. Pardakhti, M. Salavati-Niasari, Synthesis and in vitro evaluation of a novel magnetic drug delivery system; proecological method for the preparation of CoFe2O4 nanostructures, J. Mol. Liq. 249 (2018) 1151–1160, https://doi.org/10.1016/j.molliq.2017.11.133.

[29] J. Mittal, A. Batra, A. Singh, M.M. Sharma, Phytofabrication of nanoparticles through plant as nanofactories, Adv. Nat. Sci. Nanosci. Nanotechnol. 5 (2014) 43002.

[30] K.B. Gawande, S.B. Gawande, S.R. Thakare, V.R. Mate, S.R. Kadam, B.B. Kale, M. V. Kulkarni, Effect of zinc:cobalt composition in ZnCo2O4 spinels for highly selective liquefied petroleum gas sensing at low and high temperatures, RSC Adv. 5 (2015) 40429–40436, https://doi.org/10.1039/c5ra03960f.

[31] U. Holzwarth, N. Gibson, The Scherrer equation versus the "Debye-Scherrer equation", Nat. Nanotechnol. 6 (2011) 534, https://doi.org/10.1038/nnano.2011.145.

[32] T. Pandiyarajan, B. Karthikeyan, Optical properties of annealing induced post growth ZnO:ZnFe 2O4 nanocomposites, Spectrochim. Acta - Part A Mol. Biomol. Spectrosc. 106 (2013) 247–252, https://doi.org/10.1016/j.saa.2012.12.077.

[33] C. Wang, E. Shen, E. Wang, L. Gao, Z. Kang, C. Tian, Y. Lan, C. Zhang, Controllable synthesis of ZnO nanocrystals via a surfactant-assisted alcohol thermal process at a low temperature, Mater. Lett. 59 (2005) 2867–2871, https://doi.org/10.1016/j.matlet.2005.04.031.

[34] H. Ezoji, M. Rahimnejad, Electrochemical determination of Bisphenol A on multi-walled carbon nanotube/titanium dioxide-modified carbon paste electrode, Int. J. Sci. Eng. Res. 7 (2016) 242–246.
[35] Z. Zheng, J. Liu, M. Wang, J. Cao, L. Li, C. Wang, N. Feng, Selective sensing of bisphenol A and bisphenol S on platinum/poly(diallyl dimethyl ammonium chloride)-diamond powder hybrid modified glassy carbon electrode, J. Electrochem. Soc. 163 (2016) B192–B199, https://doi.org/10.1149/2.0281606jes.
[36] J. Peng, Y. Feng, X.X. Han, Z.N. Gao, Simultaneous determination of bisphenol A and hydroquinone using a poly(melamine) coated graphene doped carbon paste electrode, Microchim. Acta 183 (2016) 2289–2296, https://doi.org/10.1007/s00604-016-1865-9.
[37] X. Dong, X. Qi, N. Liu, Y. Yang, Y. Piao, Direct electrochemical detection of bisphenol a using a highly conductive graphite nanoparticle film electrode, Sensors (Switzerland) 17 (2017) 836, https://doi.org/10.3390/s17040836.
[38] P. Mohamadzadeh Jahani, S. Tajik, R. Alizadeh, M. Mortazavi, H. Beitollahi, Highly electrocatalytic oxidation of bisphenol A at glassy carbon electrode modified with metal-organic framework MOF-508a and its application in real sample analysis, Anal. Bioanal. Chem. Res. 7 (2020) 161–170.
[39] X. Wang, Y. Shi, J. Shan, H. Zhou, M. Li, Electrochemical sensor for determination of bisphenol A based on MOF-reduced graphene oxide composites coupled with cetyltrimethylammonium bromide signal amplification, Ionics (Kiel) (2020) 1–12, https://doi.org/10.1007/s11581-019-03260-6.
[40] H. Beitollahi, H. Mahmoudi Moghaddam, S. Tajik, Voltammetric determination of bisphenol A in water and juice using a lanthanum (III)-doped cobalt (II, III) nanocube modified carbon screen-printed electrode, Anal. Lett. 52 (2019) 1432–1444, https://doi.org/10.1080/00032719.2018.1545132.
[41] P. Mohammadzadeh Jahani, H. Beitollahi, S. Tajik, H. Tashakkorian, Selective electrochemical determination of bisphenol A via a Fe3O4 NPs derivative-modified graphite screen-printed electrode, Int. J. Environ. Anal. Chem. (2019) 1–17, https://doi.org/10.1080/03067319.2019.1651299.
[42] K. Shim, J. Kim, M. Shahabuddin, Y. Yamauchi, M.S.A. Hossain, J.H. Kim, Efficient wide range electrochemical bisphenol-A sensor by self-supported dendritic platinum nanoparticles on screen-printed carbon electrode, Sensors Actuators, B Chem. 255 (2018) 2800–2808, https://doi.org/10.1016/j.snb.2017.09.096.
[43] F. Wang, J. Yang, K. Wu, Mesoporous silica-based electrochemical sensor for sensitive determination of environmental hormone bisphenol A, Anal. Chim. Acta 638 (2009) 23–28, https://doi.org/10.1016/j.aca.2009.02.013.